Accepted Manuscript

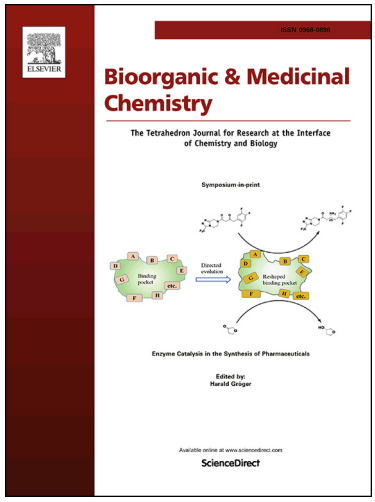

Discovery and structural characterization of peficitinib (ASP015K) as a novel and potent JAK inhibitor

Hisao Hamaguchi, Yasushi Amano, Ayako Moritomo, Shohei Shirakami, Yutaka Nakajima, Kazuo Nakai, Naoko Nomura, Misato Ito, Yasuyuki Higashi, Takayuki Inoue

PII: S0968-0896(18)31300-2
DOI: https://doi.org/10.1016/j.bmc.2018.08.005
Reference: BMC 14492

To appear in: *Bioorganic & Medicinal Chemistry*

Received Date: 20 July 2018
Revised Date: 3 August 2018
Accepted Date: 3 August 2018

Please cite this article as: Hamaguchi, H., Amano, Y., Moritomo, A., Shirakami, S., Nakajima, Y., Nakai, K., Nomura, N., Ito, M., Higashi, Y., Inoue, T., Discovery and structural characterization of peficitinib (ASP015K) as a novel and potent JAK inhibitor, *Bioorganic & Medicinal Chemistry* (2018), doi: https://doi.org/10.1016/j.bmc.2018.08.005

Discovery and structural characterization of peficitinib (ASP015K) as a novel and potent JAK inhibitor

Hisao Hamaguchi,[*] Yasushi Amano, Ayako Moritomo, Shohei Shirakami, Yutaka Nakajima, Kazuo Nakai, Naoko Nomura, Misato Ito, Yasuyuki Higashi, Takayuki Inoue[*]

Drug Discovery Research, Astellas Pharma Inc., 21, Miyukigaoka, Tsukuba, Ibaraki 305-8585, Japan

[*]Corresponding authors:

H. Hamaguchi

Tel.: +81 29 829 6193; Fax: +81 29 854 1519

E-mail: hisao.hamaguchi@astellas.com

T. Inoue

Tel.: +81 75 325 3221; Fax: +81 75 325 3222

E-mail: inoue_eck@mii.maruho.co.jp

[†]Present address: Maruho Co., Ltd, Bldg. 5, Kyoto Research Park, 93 Awata-cho, Chudoji, Shimogyo-ku, Kyoto 600-8815, Japan

Abstract

Janus kinases (JAKs) are considered promising targets for the treatment of autoimmune diseases including rheumatoid arthritis (RA) due to their important role in multiple cytokine receptor signaling pathways. Recently, several JAK inhibitors have been developed for the treatment of RA. Here, we describe the identification of the novel orally bioavailable JAK inhibitor **18**, peficitinib (also known as ASP015K), which showed moderate selectivity for JAK3 over JAK1, JAK2, and TYK2 in enzyme assays. Chemical modification at the C4-position of lead compound **5** led to a large increase in JAK inhibitory activity and metabolic stability in liver microsomes. Furthermore, we determined the crystal structures of JAK1, JAK2, JAK3, and TYK2 in a complex with peficitinib, and revealed that the 1*H*-pyrrolo[2,3-*b*]pyridine-5-carboxamide scaffold of peficitinib forms triple hydrogen bonds with the hinge region. Interestingly, the binding modes of peficitinib in the ATP-binding pockets differed among JAK1, JAK2, JAK3, and TYK2. WaterMap analysis of the crystal structures suggests that unfavorable water molecules are the likely reason for the difference in orientation of the 1*H*-pyrrolo[2,3-*b*]pyridine-5-carboxamide scaffold to the hinge region among JAKs.

Keywords

peficitinib, ASP015K, JAK (Janus kinase), JAK inhibitor, immunomodulator, crystal structures, WaterMap, rheumatoid arthritis

1. Introduction

Rheumatoid arthritis (RA) is one of the most common chronic inflammatory autoimmune diseases; it targets synovial tissues and causes progressive joint disability.[1] Over the past decades, disease-modifying anti-rheumatic drugs (DMARDs) like methotrexate (MTX), which is the anchor drug in RA therapy, have formed the basis of RA treatments. Several approved biological agents, including tumor necrosis factor antagonists, T-cell co-stimulation blockade and interleukin (IL)-6 receptor antagonists, have been shown to be effective in patients who had poor response to conventional DMARDs.[1-3] However, the disadvantages of these current drugs, such as inconvenient routes of administration, side effects such as serious infection, and lack or loss of efficacy due to anti-drug antibody production, warrant additional treatment options for RA.[1,4] Therefore, there is still a significant unmet need for orally available small molecules with improved efficacy.[5,6]

JAKs are a family of cytoplasmic protein tyrosine kinases with four known members (JAK1, JAK2, JAK3, and TYK2) that are associated with various cytokine-mediated signal transduction pathways.[7-9] Binding of the ligands to their corresponding receptors induces JAK activation and subsequent phosphorylation of the receptors. Subsequently, the activated JAKs phosphorylate signal

transducers and activators of transcription (STAT) proteins, which form dimers, translocate to the nucleus, and promote cytokine-responsive gene expression.[10-12]

In the JAK family, JAK3 is selectively expressed in hematopoietic cells, while the other three members are ubiquitously expressed.[13-15] JAK3 is specifically associated with common γ-chain (γc) cytokines such as IL-2, IL-4, IL-7, IL-9, IL-15, and IL-21, which play key roles in T-cell differentiation, proliferation, and survival.[7-12] In addition, JAK3 knockout mice exhibit severe combined immunodeficiency but no other remarkable phenotypes.[16,17] JAK1 is also linked to the IL-2 receptor and regulates T cell proliferation in concert with JAK3. Additionally, JAK1 is associated with the signaling pathways of IL-6 and interferon (IFN)-γ for inflammatory responses in psoriasis and RA.[7-12] In contrast, JAK2 has the most characteristic profile of the four JAK kinases. JAK2 mediates signaling of hematopoietic growth factors such as erythropoietin (EPO) and thrombopoietin, and JAK2-knockout mice are embryonic lethal because of defective erythropoiesis.[7,11] Therefore, JAK2 inhibition may affect some essential functions regulated by EPO.[18] TYK2 has been shown to regulate the cytokine-mediated signals of IFN-α, IL-12, IL-23, which are related to psoriasis and inflammatory bowel disease.[19,20]

To date, a number of JAK inhibitors have been developed for the treatment of RA.[21,22] Tofacitinib (compound **1**, Figure 1) was the first developed small molecule JAK inhibitor, and was approved in 2012 as a pan JAK inhibitor for the treatment of RA.[23,24] Most recently, the JAK1 and JAK2 inhibitor baricitinib (compound **2**, Figure 1) was approved in the EU as a monotherapy or in combination with MTX for patients with RA not responding adequately to one or more DMARDs.[25] Further, specific JAK1 inhibitors filgotinib and upadacitinib (compound **3** and compound **4**, respectively, Figure 1) are currently being evaluated in clinical trials for RA.[26,27]

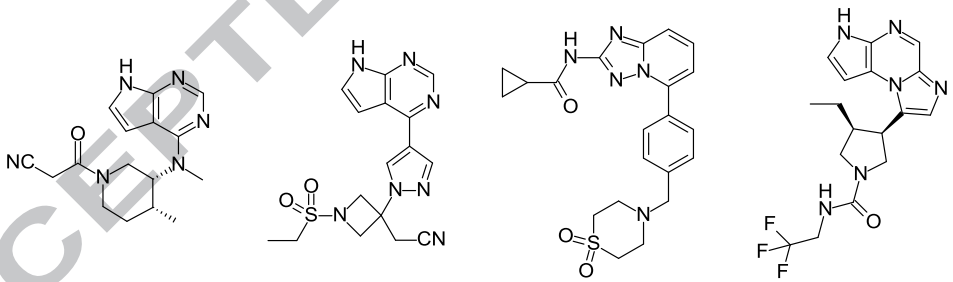

Figure 1. Chemical structures of tofacitinib **1,** baricitinib **2**, filgotinib **3** and upadacitinib **4**.

In our previous research, 1*H*-pyrrolo[2,3-*b*]pyridine-5-carboxamide derivative **5** was identified as a lead compound and a potent and moderately selective JAK3 inhibitor (Figure 2).[28] However, lead compound **5** showed poor metabolic stability in liver microsomes and in vivo Pharmacokinetic (PK) profiles due to high molecular lipophilicity. Additionally, docking calculations to JAK3 indicated that the pyrrolopyridine scaffold of **5** interacted with the hinge region of the ATP-binding site and that the C4-substituent of the pyrrolopyridine ring occupied the hydrophobic cavity.[28]

Here, we report the design, synthesis, and structural characterization of a novel JAK inhibitor with moderate selectivity for JAK3 inhibition, peficitinib (ASP015K), as alternative option for the treatment of RA.

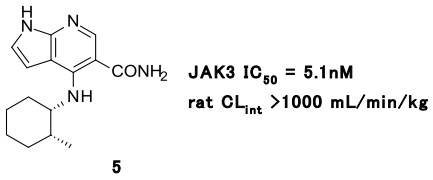

Figure 2. Chemical structure of lead compound **5**.

2. Chemistry

1*H*-Pyrrolo[2,3-*b*]pyridine-5-carboxamide derivatives were synthesized as shown in Scheme 1. Compound **6** was prepared as previously described.[28] Nucleophilic substitution of the chloride at the C4-position with several amines under microwave irradiation yielded the desired compounds **7a–c**.

Aminoadamantane derivatives were synthesized as summarized in Scheme 2. 4-Aminoadamantan-1-ol **8**[29] was protected with benzyl chloroformate (CbzCl). The diastereomers were chromatographically separated to obtain *trans*-isomer **9** and *cis*-isomer **10**. Removal of the Cbz group of **9** and **10** by Pd-catalyzed hydrogenation gave the corresponding *trans*-4-aminoadamantan-1-ol **11** and *cis*-4-aminoadamantan-1-ol **12**.[30] *Trans*-5-fluoroadamantan-2-amine **14** was obtained by fluorination of the hydroxyl group of compound **9** by treating with bis(2-methoxyethyl)aminosulfur trifluoride (Deoxo-Fluor) and subsequent deprotection of the Cbz group. *Trans*-5-methoxyadamantan-2-amine **16** was synthesized by methylation of the hydroxyl group of **9** with trimethyloxonium tetrafluoroborate and subsequent deprotection of the Cbz group.

Compounds **17a–d** and **18** were synthesized as outlined in Scheme 3. In a similar manner to Scheme 1, compound **6** was treated with aminoadamantane derivatives to give the corresponding C4-substituted compounds **17a–d**.

Furthermore, **17a** was treated with 48% hydrobromic acid to obtain hydrobromide salt **18**.

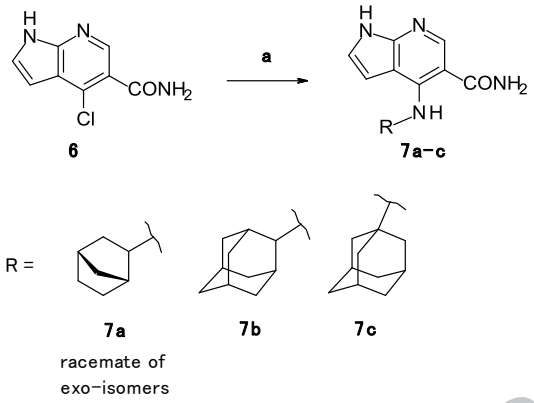

Scheme 1. Reagents and conditions: (a) amine, $Et_3N{\cdot}HCl$, DMI, microwave, 160 °C or amine, Et_3N, NMP, microwave, 180-200 °C.

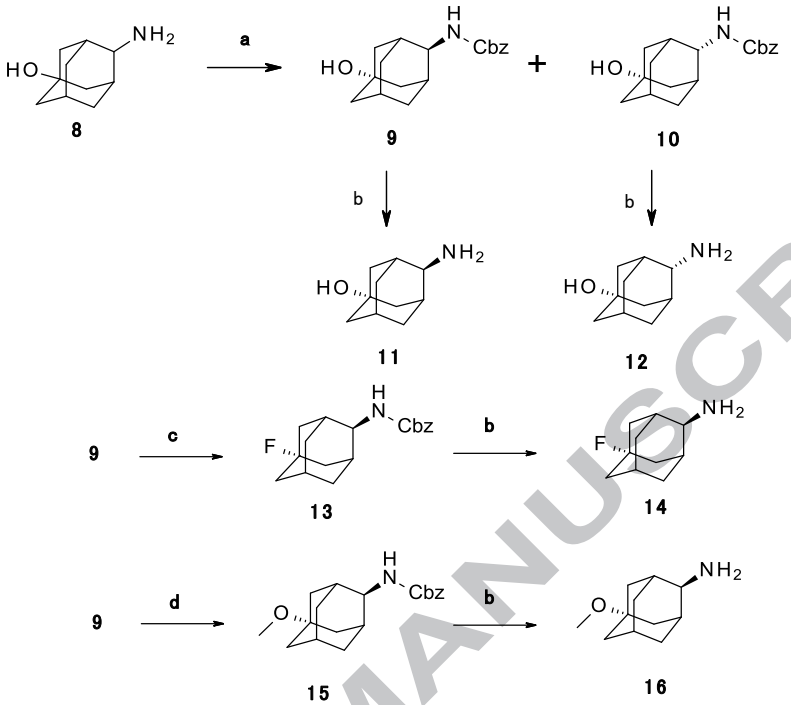

Scheme 2. Reagents and conditions: (a) CbzCl, 1 M NaOH aq., THF, 0 °C; (b) H_2, 10% Pd/C (50% wet), MeOH, room temperature; (c) Deoxo-Fluor, CH_2Cl_2, 0 °C; (d) Trimethyloxonium tetrafluoroborate, 2,6-di-*t*-butyl-4-methylpyridine, DCE, 95 °C.

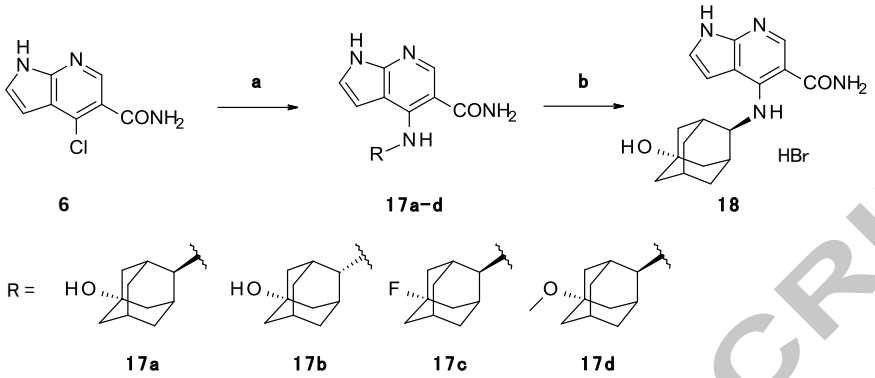

Scheme 3. Reagents and conditions: (a) amine, Et_3N, NMP, microwave, 200 °C or amine, *n*-Bu_3N, NMP, 200 °C; (b) 48% HBr aq., EtOAc, reflux.

3. Results and Discussion

3.1. In vitro structure-activity relationships (SARs)

As JAK3 and JAK1 collaboratively regulate the IL-2 signaling pathway, we evaluated our newly synthesized compounds for human JAK3 and JAK1 inhibitory activity. We also investigated JAK2 inhibitory activity because it is potentially associated with hematopoietic side effects such as anemia.[31] Additionally, we also evaluated the compounds' metabolic stability in rat liver microsomes.

As shown in Table 1, lead compound 1*H*-pyrrolo[2,3-*b*]pyridine-5-carboxamide derivative **5** showed potent JAK3 inhibitory activity (IC_{50} = 5.1 nM) and moderate T cell proliferation inhibitory activity (IC_{50} = 86 nM).[28] To increase JAK3 inhibitory activity, we focused on further optimizing the C4-substituent of **5**. As we previously reported, docking calculations of lead compound **5** to human JAK3 indicated that the cyclohexane ring was directed towards the hydrophobic cavity, and WaterMap analysis showed that the bulkiness of the C4-substituent was linked to JAK3 inhibitory activity.[28] Therefore, to enhance the affinity of the hydrophobic cavity, we investigated the conversion of the C4-cyclohexane ring of **5** to a bridged ring. As we expected, norbornane derivative **7a** had increased potency for JAK3 (IC_{50} = 3.2 nM) and JAK1 (IC_{50} = 24 nM), indicating that

bridging the cyclohexane ring increases JAK inhibitory activity. We therefore next evaluated adamantane derivatives **7b** and **7c**, which had the most highly bridged rings. Conversion of the C4-cyclohexane ring to 2-adamantane derivative **7b** effectively increased JAK3 and JAK1 inhibition (IC_{50} = 2.1 nM and IC_{50} = 12 nM, respectively). Unfortunately, 1-adamantane derivative **7c** showed a slight decrease in JAK3 inhibitory activity (IC_{50} = 10 nM) compared to **5**. From these results, **7b** was selected for further chemical modification.

Interestingly, although the microsomal intrinsic clearance (CL_{int}) of **7b** was high (>1000 mL/min/kg) because of high molecular lipophilicity (*C*logP = 5.11), the metabolic stability of **7a** was slightly better than that of **5** due to the reduction in molecular lipophilicity (*C*logP = 4.12). This result suggests that reducing molecular lipophilicity is effective for improving metabolic stability. In addition, in our previous study, we reported that the conversion of methyl group of **5** to hydroxymethyl group showed reduced metabolic clearance and improved oral absorption compared to **5**.[28] Therefore, we next investigated the effect of introducing a polar functional group to the C4-adamantyl moiety to decrease the molecular lipophilicity of **7b**.

Table 1. SAR of modifying the cyclohexane ring moiety in the C4-substituent

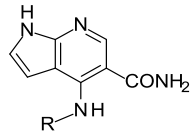

Compound	R	JAK3 IC_{50} (nM)[a]	JAK1 IC_{50} (nM)[a]	JAK2 IC_{50} (nM)[a]	T cells IC_{50} (nM)[b]	*In vitro* CL_{int}[c] (mL/min/kg)	*C*logP[d]
5	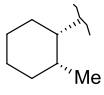 chiral	5.1	47	30	86	>1000	4.76
7a	 racemate of exo -isomers	3.2	24	15	NT[e]	859	4.12
7b	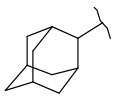	2.1	12	11	NT[e]	>1000	5.11
7c	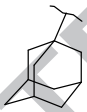	10	110	120	NT[e]	NT[e]	5.09

[a,b]Experiments were performed in duplicate. [b]The inhibitory effect on IL-2-stimulated T cell proliferation using rat spleen cells. [c]*In vitro* metabolism with rat liver microsomes in the presence of NADPH. [d]*C*LogP values were calculated using ACD/Percepta, version 2016.2. [e]NT = not tested.

To introduce a polar functional group to the adamantyl moiety, we first performed a docking calculation for **7b** to human JAK3 (PDB code: 3LXK[32]) (Figure 3). The predicted binding mode of **7b** was similar to that of **5,** and suggested that the adamantyl moiety would occupy the hydrophobic cavity and that polar residues such as Arg953 and Asp967 exist around it. From this result, we expected that introducing a hydroxyl group to the C5-position of the 2-adamantyl moiety would lead to the formation of a hydrogen bond between polar residues.

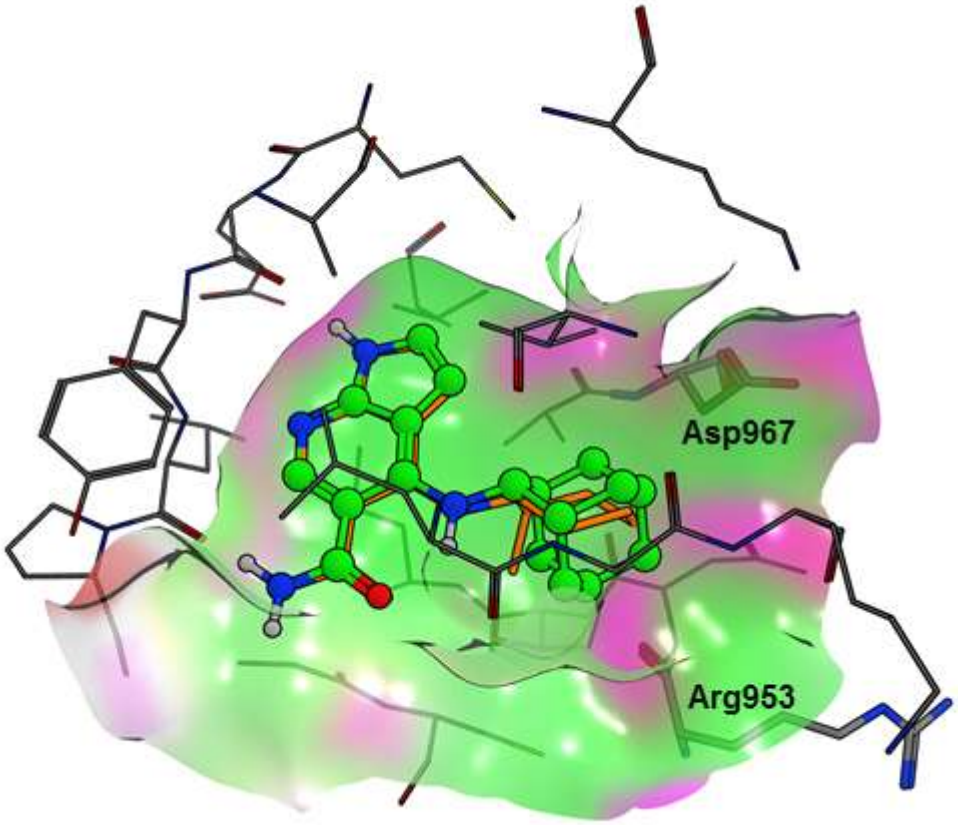

Figure 3. Predicted binding mode of compound **7b** (green) and **5** (orange) to human JAK3.

As shown in Table 2, we investigated various 2-adamantane derivatives for human JAK1, JAK2 and JAK3 inhibitory activity and metabolic stability using rat liver microsomes. First, we examined the effect of introducing a hydroxyl group to the C4-adamantane ring. As we expected from docking study (Figure 3), compound **17b** showed highly potent JAK inhibitory activity (JAK3, JAK1, and JAK2 IC_{50} = 0.43, 0.49, and 1.7 nM, respectively). *Trans*-isomer **18** of **17b** also showed potent JAK3 inhibitory activity and moderate selectivity for JAK3 (JAK3, JAK1, and JAK2 IC_{50} = 0.71, 3.9, and 5.0 nM, respectively). Subsequent testing of the metabolic stability of compounds **17b** and **18** using rat liver microsomes showed good metabolic stability (CL_{int} = 199 mL/min/kg and 124 mL/min/kg, respectively) due to the reduced lipophilicity (*C*logP = 3.26). Our calculations also suggested that the introduction of fluoro and methoxy groups should reduce the molecular lipophilicity compared to that of **7b** (*C*logP = 4.42 and 3.90, respectively). We therefore examined the metabolic blocking effect of fluoro and methoxy groups using *trans*-isomer **18** because of its lower potency for JAK2 inhibitory activity than **17b**. As a result, **17c** showed equivalent JAK3 inhibitory activity (IC_{50} = 2.1 nM) to **7b**, and **17d** showed a 3-fold increase in JAK3 inhibitory activity (IC_{50} = 0.63 nM) compared to **7b**. However, the metabolic stability of neither **17c** nor **17d** was improved (CL_{int} >1000 mL/min/kg). These

results suggested that a polar moiety such as the hydroxyl group was necessary for metabolic stability; therefore, **18** (peficitinib, ASP015K) was chosen for further biological evaluation. Additionally, **18** showed high metabolic stability in human liver microsomes (CL_{int} = 26 mL/min/kg).

Table 2. SAR of 2-adamantane derivatives

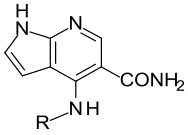

Compound	R	JAK3 IC_{50} (nM)[a]	JAK1 IC_{50} (nM)[a]	JAK2 IC_{50} (nM)[a]	*In vitro* CL_{int}[b] (mL/min/kg)	*C*logP[c]
7b	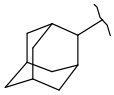	2.1	12	11	>1000	5.11
17b	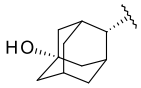	0.43	0.49	1.7	199	3.26
18[d]	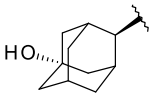	0.71 (0.38–1.4)	3.9 (2.1–7.2)	5.0 (3.7–6.9)	124	3.26
17c	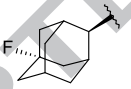	2.1	19	11	>1000	4.42
17d	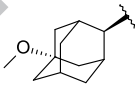	0.63	7.8	5.0	>1000	3.90

[a]Experiments were performed in duplicate. [b]*In vitro* metabolism with rat liver microsomes in the presence of NADPH. [c]*C*LogP values were calculated using ACD/Percepta, version 2016.2. [d]IC_{50} values for each assay indicate the average of four independent experiments with 95% confidence intervals in parentheses.

The results of nonclinical pharmacology studies of peficitinib are shown in Table 3. Peficitinib inhibited JAK activity with IC_{50} values of 3.9 nM (JAK1), 5.0 nM (JAK2), 0.71 nM (JAK3), and 4.8 nM (TYK2), showing moderate selectivity for JAK3. In addition, peficitinib inhibited IL-2-induced rat and human T cell proliferation with similar potency (IC_{50} = 10 and 18 nM, respectively). Furthermore, peficitinib prevented EPO-induced proliferation of the human erythroleukemia cell line TF-1 (IC_{50} = 248 nM), which involves JAK2 activity, with 14-fold less potency than that against human T cell proliferation. This milder inhibition of JAK2 by peficitinib may contribute to the alleviation of JAK2-mediated adverse hematopoietic effects.

Table 3. Inhibition of Janus kinases and cell proliferation by peficitinib (**18**)

JAK1 IC_{50} (nM)[a]	JAK2 IC_{50} (nM)[a]	JAK3 IC_{50} (nM)[a]	TYK2 IC_{50} (nM)[b]	Rat T cells IC_{50} (nM)[a]	Human T cells IC_{50} (nM)[a]	Human TF-1 IC_{50} (nM)[a]
3.9 (2.1–7.2)	5.0 (3.7–6.9)	0.71 (0.38–1.4)	4.8 (NA)	10[c] (7.1–14.5)	18[d] (6.8-49)	248[e] (192-320)

[a]IC_{50} values for each assay indicate the average of four independent experiments with 95% confidence intervals in parentheses. [b]95% confidence intervals are not applicable (NA) for TYK2 because only one experiment was conducted. [c]The inhibitory effect on IL-2-stimulated T cell proliferation using rat spleen cells. [d]The inhibitory effect on IL-2-stimulated T cell proliferation using human peripheral blood mononuclear cells. [e]The inhibitory effect on EPO-induced proliferation of the human erythroleukemia cell line TF-1.

3.2. PK profile

PK study of peficitinib was performed in rats, and the results following oral (po) and intravenous (iv) administration are shown in Table 4. Peficitinib showed good oral bioavailability (45.9%). Moreover, we previously reported that peficitinib showed dose-dependent efficacy by oral administration in prophylactic and therapeutic dosing regimens in an adjuvant-induced arthritis rat model.[33] These data suggest that peficitinib may be a potentially effective therapy for the oral treatment of RA and other autoimmune disorders.

Table 4. Pharmacokinetic parameters of peficitinib (**18**) in rats after oral and intravenous administration[a]

	Dose (mg/kg)	C_{max} (ng/mL)	t_{max} (h)	$AUC_{0-\infty}$ (ng·h/mL)	$t_{1/2}$ (h)	CL_{tot} (L/h/kg)	Vdss (L/kg)	*F* (%)[b]
po	1	125.67	0.25	263.67	2.12	—	—	45.9
iv	1	—	—	574.52	4.72	1.74	1.83	—

[a]Pharmacokinetic parameters were determined from mean plasma concentrations (n=3) at each time-point. [b]*F* = Bioavailability.

3.3. Crystal structures of JAK1, JAK2, JAK3, and TYK2 in a complex with peficitinib ***18***

To confirm the binding modes of peficitinib in co-crystal structures with JAK kinases, we determined the crystal structures of JAK1, JAK2, JAK3, and TYK2 in a complex with peficitinib.

In the complex structure with JAK1, peficitinib bound the ATP-binding site of JAK1 as expected (Figure 4). The pyrrolopyridine ring inserted into the planar pocket along the hinge region, where it formed two hydrogen bonds with the main chain atoms of Glu957 (3.1 Å) and Leu959 (3.2 Å). The carbamoyl group formed a hydrogen bond with the main chain atom of Leu959 (3.3 Å). In addition, the carbamoyl group formed hydrogen bonds with two water molecules, which formed hydrogen bonds with Pro960, Glu966, and Ser963. The carbamoyl group also formed an internal hydrogen bond with the C4 amino group of the pyrrolopyridine ring. The adamantyl group occupied the large cavity adjacent to the planar pocket and formed a hydrophobic interaction with Val889. Further, the hydroxyl group was located inside the pocket and formed a hydrogen bond with Asn1008.

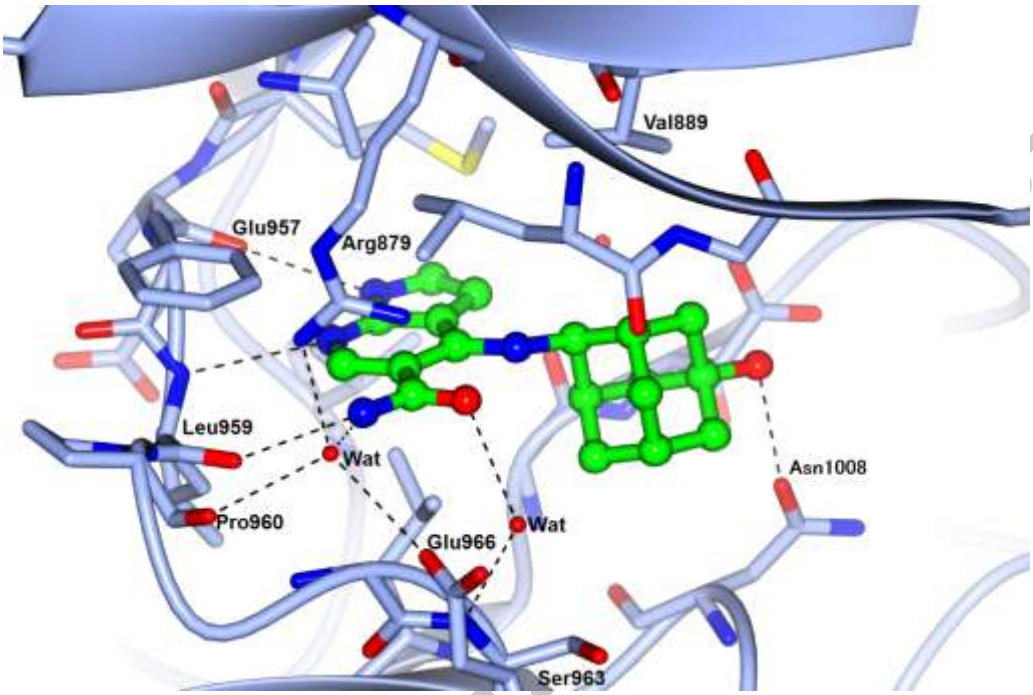

Figure 4. Crystal structure of JAK1 in a complex with peficitinib (PDB code: 6AAH).[36.] JAK1 is depicted as the light blue ribbon and stick model. Peficitinib is depicted as the green ball and stick model. Water molecules are depicted as red balls.

In the complex structure with JAK2, as for JAK1, peficitinib bound the ATP-binding site (Figure 5). Surprisingly, peficitinib was flipped compared to the JAK1 complex structure; that is, the carbamoyl group was inside the pocket and the pyrrolopyridine ring pointed outside the pocket. At the hinge region, the carbamoyl group and the N7 atom of the pyrrolopyridine ring formed hydrogen bonds with the main chain atom of Glu930 (2.8 Å) and Leu932 (3.2 Å), respectively. The N1 atom of the pyrrolopyridine ring formed a weak hydrogen bond with the main chain oxygen atom of Leu932 (3.5 Å). The adamantyl group occupied the large cavity and formed a hydrophobic interaction with Val863, as in the JAK1 complex. In contrast, the hydroxyl group of the adamantyl moiety was located close the solvent region and did not form any polar interactions with amino acid residues.

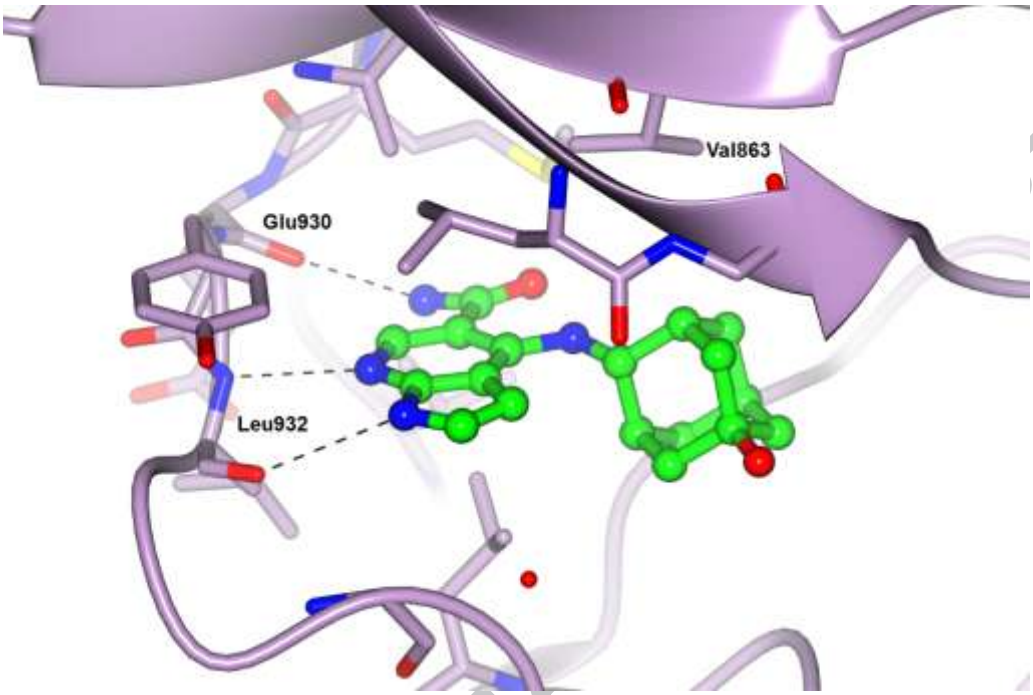

Figure 5. Crystal structure of JAK2 in a complex with peficitinib (PDB code: 6AAJ). JAK2 is depicted as the light purple ribbon and stick model. Peficitinib is depicted as the green ball and stick model. Water molecules are depicted as red balls.

In the complex structure with JAK3, peficitinib showed a similar binding mode to that observed for the JAK2 complex (Figure 6). However, the distances of hydrogen bonds with the hinge region differed slightly. With JAK3, the pyrrolopyridine ring formed two hydrogen bonds with the main chain atoms of Leu905 (3.4 and 3.1 Å), and the carbamoyl group formed a hydrogen bond with the main chain atom of Glu903 (3.4 Å) in the hinge region. The oxygen atom of the carbamoyl group formed a hydrogen bond with a water molecule that bound the main chain atom of Asp967 and an internal hydrogen bond with the C4 amino group of the pyrrolopyridine ring, as in the JAK1 structure. The hydroxyl group of the adamantyl moiety formed a hydrogen bond with a water molecule that bound the main chain atom of Arg953. Although this binding mode was different to that predicted by docking study of **7b** (Figure 3), peficitinib showed high JAK3 inhibitory activity by interacting through this water molecule. This suggests that the two water molecules that bind the main chain atom of Asp967 or Arg953 are involved in the interaction between JAK3 and peficitinib. As the coordinates of residues around these water molecules are well conserved between JAK2 and JAK3, it is likely that JAK2 also interacts with the carbamoyl and hydroxyl groups via water molecules, which were not observed due to the relatively low resolution. Therefore, the introduction of a hydroxyl group to the C5-position of

the 2-adamantyl moiety may contribute to the increase in JAK1, JAK2 or JAK3 inhibitory activity observed for peficitinib compared to compound **7b** regardless of direct or indirect interactions via water molecules.

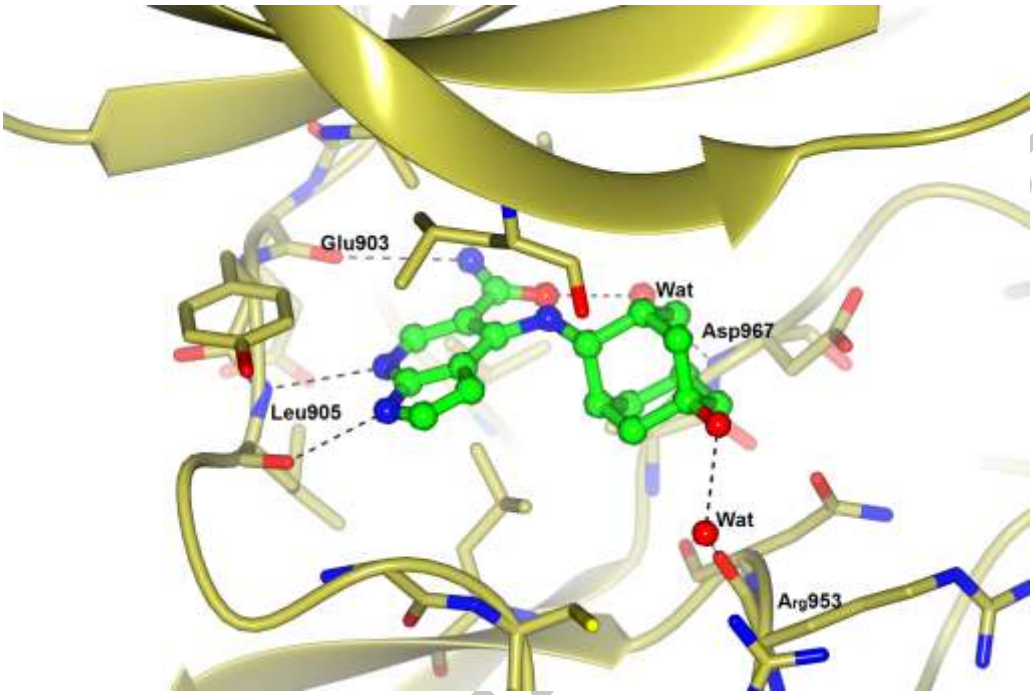

Figure 6. Crystal structure of JAK3 in a complex with peficitinib (PDB code: 6AAK).[36.] JAK3 is depicted as the light brown ribbon and stick model. Peficitinib is depicted as the green ball and stick model. Water molecules are depicted as red balls.

In the complex structure with TYK2, peficitinib showed a unique binding mode (Figure 7). The pyrrolopyridine ring formed two hydrogen bonds with the main chain atoms of Val981 (2.9 and 2.8 Å), and the carbamoyl group formed a hydrogen bond with the main chain atom of Glu979 (3.1 Å) in the hinge region. The oxygen atom of the carbamoyl group formed a hydrogen bond with a water molecule that bound the main chain atom of Asp1041, similar to that observed for the JAK3 structure. In addition, the hydroxyl group formed hydrogen bonds with the side chains of Asp1041 and Asn1028. Therefore, the binding mode of the pyrrolopyridine ring to the hinge region in TYK2 is similar to that in the JAK2 and JAK3 structures, while the binding mode of the adamantyl moiety is same as that in the JAK1 structure.

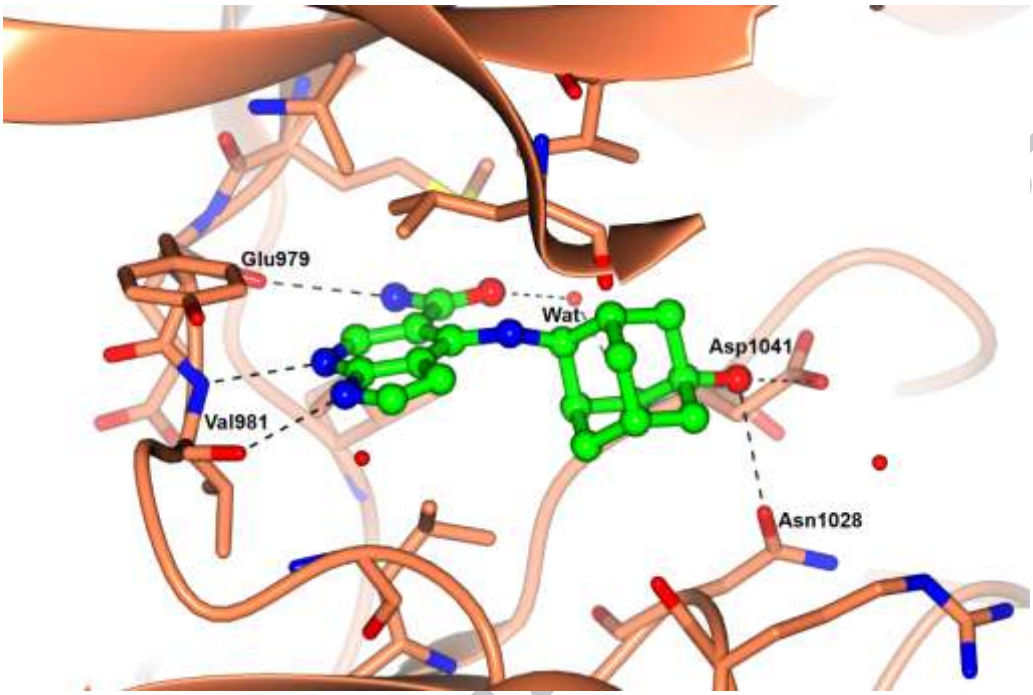

Figure 7. Crystal structure of TYK2 in a complex with peficitinib (PDB code: 6AAM). TYK2 is depicted as the orange ribbon and stick model. Peficitinib is depicted as the green ball and stick model. Water molecules are depicted as red balls.

3.4. WaterMap analysis

The co-crystal structures of peficitinib with JAKs indicated that the orientation of the 1*H*-pyrrolo[2,3-*b*]pyridine-5-carboxamide scaffold with respect to the hinge region differed between JAK1 and the other JAK proteins (JAK2, JAK3, and TYK2). To examine this difference, we carried out WaterMap analysis of the X-ray co-crystal structures. WaterMap is a program to quantitatively estimate the dehydration effect with the ligand and receptor binding.[34,35]

Each WaterMap analysis results are shown in Figure 8, and superimposed results is shown in Figure 9. As we previously reported, there are 1*H*-pyrrolo[2,3-*b*]pyridine-5-carboxamide scaffold site and C4-substituent site in JAK3 ligand binding pocket [28] and similar results were found in this time WaterMap analyses. The WaterMap results suggest that peficitinib effectively displaced unfavorable water molecules in JAK1, JAK2, JAK3, and TYK2 (Figure 8). For more details, there are five unfavorable water molecules at the 1*H*-pyrrolo[2,3-*b*]pyridine-5-carboxamide scaffold site (Figure 9B) and their positions are overlapped and can be divided into 2 groups kinase hinge region G1 and G2 based on their position.

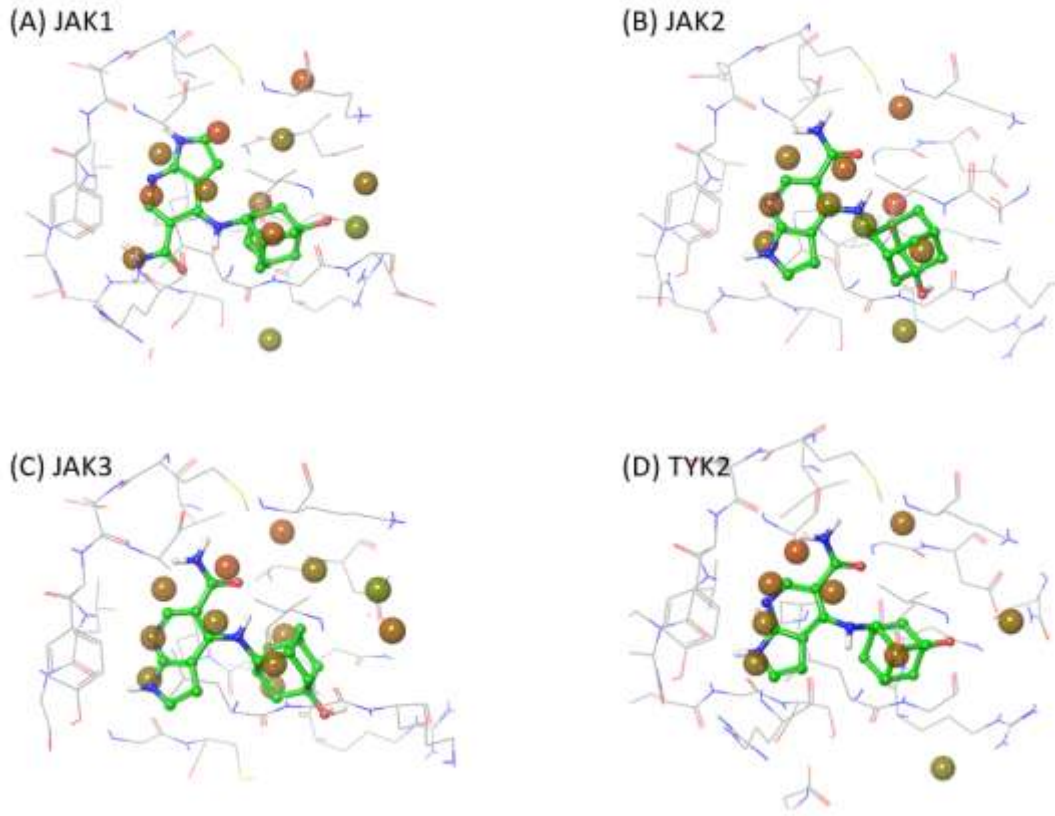

Figure 8. Peficitinib (light green) with WaterMap unfavorable water molecules ($\Delta G \geq 2.0$ kcal/mol, within 5Å of peficitinib). (A) JAK1, (B) JAK2, (C) JAK3, (D) TYK2. WaterMap hydration sites are presented as spheres, and color is based on the calculated ΔG. Unfavorable sites are shown in red and favorable sites in green.

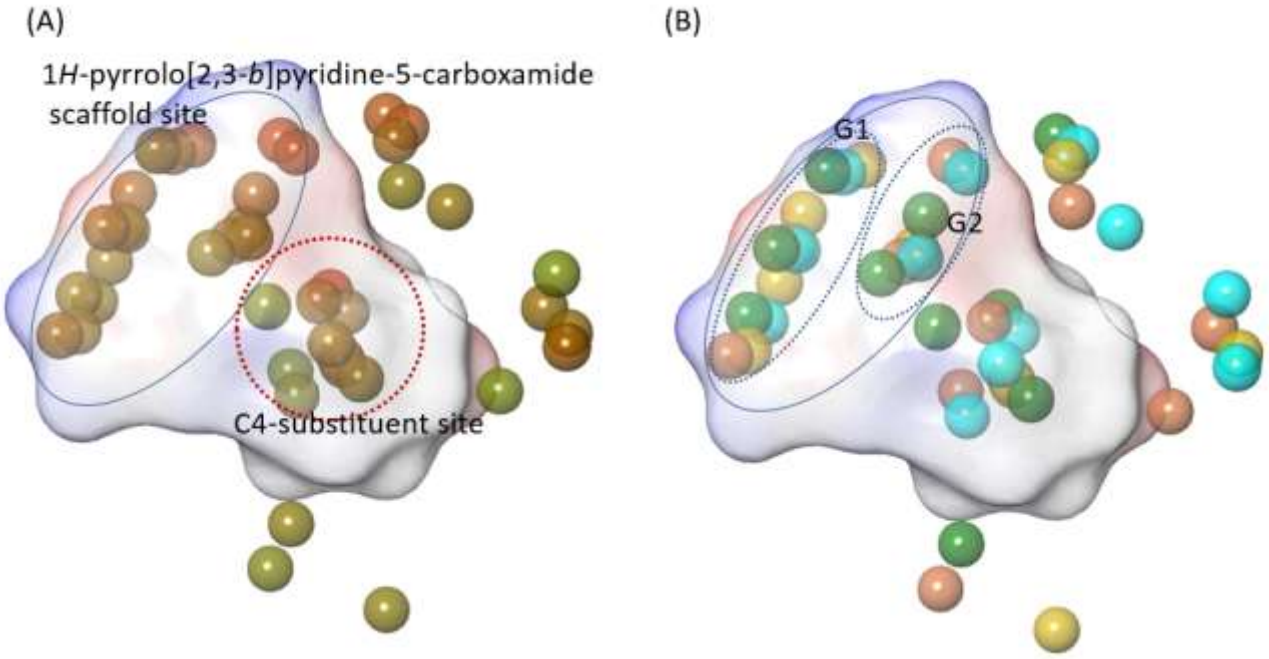

Figure 9. JAKs WaterMap Unfavorable Water Molecules ($\Delta G \geq 2.0$ kcal/mol, within 5Å of peficitinib) with Ligand surface. Water sites are colored by absolute (A), unfavorable sites are shown in red and favorable sites in green, colored by receptor (B), JAK1: orange, JAK2: green, JAK3: cyan, TYK2: yellow.

Here, we focused on the displacement of the unfavorable water molecules of G1 and G2. As shown by the orange arrows in Figure 10, two unfavorable water molecules of JAK1 are positioned at the outermost. Therefore, to effectively remove these unfavorable water molecules, we predict that the 1*H*-pyrrolo[2,3-*b*]pyridine-5-carboxamide scaffold of peficitinib must be oriented differently to JAK1 compared to the other JAK proteins (JAK2, JAK3, and TYK2).

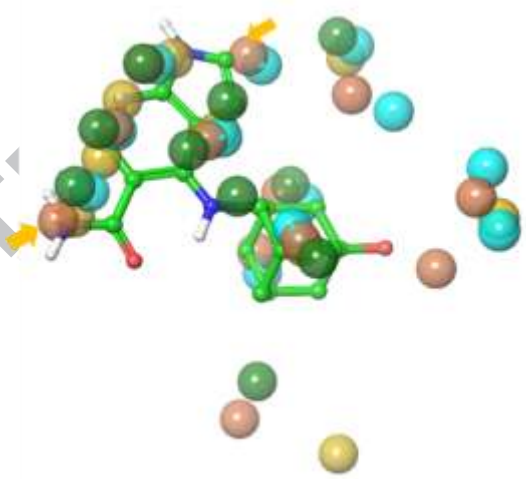

Figure 10. WaterMap Unfavorable Water Molecules ($\Delta G \geq 2.0$ kcal/mol, within 5Å of peficitinib) with peficitinib (light green). Water sites are colored by receptor. JAK1: orange, JAK2: green, JAK3: cyan, TYK2: yellow.

4. Conclusion

We investigated the effect of converting the C4-cyclohexane ring of lead compound **5** to a bridged ring, and found that the 2-adamantyl moiety played an important role in increasing JAK3 inhibitory activity. In addition, we examined the location at which a polar group is introduced to the adamantyl moiety using docking calculations for **7b** for human JAK3. We found that introducing a hydroxyl group to the C5-position of the 2-adamantyl moiety led to improved metabolic stability, and **18** (peficitinib, ASP015K) was identified as a novel orally bioavailable JAK inhibitor with moderate selectivity for JAK3 over JAK1, JAK2, and TYK2 in enzyme assays. Additionally, analysis of the co-crystal structures of peficitinib with JAK families revealed that peficitinib forms triple hydrogen bonds with the main chain atoms from hinge residues. Interestingly, the orientation of the 1*H*-pyrrolo[2,3-*b*]pyridine-5-carboxamide scaffold to the hinge region of the ATP-binding site in JAK1 was different to that of the other JAK proteins (JAK2, JAK3, and TYK2). Furthermore, WaterMap analysis of JAK families suggested that the position of unfavorable water molecules may determine the orientation of the 1*H*-pyrrolo[2,3-*b*]pyridine-5-carboxamide scaffold. Peficitinib is currently being under developmet for the treatment of RA.

5. Experimental section

5.1. Chemistry

^{1}H NMR spectra were measured using a Brucker DPX200, Avance 400, AV400M, Brucker Avance III HD500, or Varian VNS-400 spectrometer. Chemical shifts are expressed in δ units (ppm) using tetramethylsilane as an internal standard. Abbreviations of ^{1}H NMR signal patterns are as follows: s, singlet; d, doublet; t, triplet; q, quartet; m, multiplet; br, broad. Mass spectra (MS) were recorded on Agilent 1100 LC/MSD, Thermo Fisher Scientific LCQ Advantage, or Waters UPLC/SQD. Electrospray ionization positive high-resolution mass spectrum (HRMS) was performed using Thermo Scientific Exactive Plus. Column chromatography was carried out using silica gel 60N (Kanto Chemical, 63-210 μm) or HI-FLASH^{TM} Column (Yamazen). Elemental analysis values were recorded on Elementar Vario EL III (C, H, N) and Dionex ICS-3000 (S, halogene), and were within ±0.4% of theoretical values. Unless otherwise noted, all reagents and solvents were obtained from commercial suppliers and used without further purification. The following abbreviations are used: *n*-Bu_3N, *normal*-tributylamine; DCE, 1,2-dichloroethane; Deoxo-Fluor; bis(2-methoxyethyl)aminosulfur trifluoride; DMI, 1,3-dimethylimidazolidin-2-one; DMSO, dimethylsulfoxide; Et_3N, triethylamine;

Et_2O, diethyl ether; EtOAc, ethyl acetate; IPE, diisopropyl ether; MeOH, methanol; NMP, *N*-methyl-2-pyrrolidone; THF, tetrahydrofuran.

5.1.1. 4-{[2-*ambo*-(1*R*,2*R*,4*S*)-Bicyclo[2.2.1]heptan-2-yl]amino}-1*H*-pyrrolo[2,3-*b*]pyridine-5-carboxamide (7a)

A mixture of 4-chloro-1*H*-pyrrolo[2,3-*b*]pyridine-5-carboxamide (**6**) (100 mg, 0.51 mmol), *exo*-2-aminonorbornane (171 mg, 1.53 mmol), and Et_3N·HCl (70.4 mg, 0.51 mmol) in DMI (0.40 mL) was heated in a microwave reactor at 160 °C for 1 h. After cooling to room temperature, the mixture was diluted in EtOAc and a white solid was filtered off. $CHCl_3$ and EtOAc were added to the residue, and the precipitate was filtrated to give the title compound (73.2 mg, 53%). ^{1}H NMR (DMSO-d_6) δ 1.12–1.65 (m, 7H), 1.82–1.97 (m, 1H), 2.25–2.34 (m, 2H), 3.85–3.96 (m, 1H), 6.57 (d, J = 3.3 Hz, 1H), 6.78–7.99 (br, 2H), 7.12 (d, J = 2.4 Hz, 1H), 8.35 (s, 1H), 9.57 (d, J = 7.1 Hz, 1H), 11.45 (br s, 1H); MS (ESI) *m/z* 271 $[M+H]^+$; HRMS (ESI) *m/z* Calcd for $C_{15}H_{19}N_4O$ ($[M+H]^+$): 271.1553, Found: 271.1555.

5.1.2. 4-[(Adamantan-2-yl)amino]-1*H*-pyrrolo[2,3-*b*]pyridine-5-carboxamide (7b)

A mixture of **6** (40 mg, 0.20 mmol), 2-adamantanamine hydrochloride (192 mg, 1.02 mmol), and Et_3N (0.14 mL, 1.02 mmol) in NMP (0.40 mL) was heated in a

microwave reactor at 180 °C for 1 h. After cooling to room temperature, H_2O was added and the mixture was extracted with EtOAc. The organic layer was separated, washed with brine, dried over $MgSO_4$, and concentrated under reduced pressure. The residue was purified by column chromatography on silica gel ($CHCl_3$/MeOH =95/5 to 90/10). The obtained solid was washed with IPE to give the title compound (32 mg, 50%). ^{1}H NMR (DMSO-d_6) δ 1.53–1.61 (m, 2H), 1.69–1.76 (m, 2H), 1.80–2.06 (m, 10H), 4.15–4.21 (m, 1H), 6.39–6.44 (m, 1H), 6.81–7.18 (br, 1H), 7.09–7.13 (m, 1H), 7.53–7.91 (br, 1H), 8.37 (s, 1H), 10.17 (d, J = 8.0 Hz, 1H), 11.44 (br s, 1H); MS (ESI) *m/z* 311 $[M+H]^+$; HRMS (ESI) *m/z* Calcd for $C_{18}H_{23}N_4O$ ($[M+H]^+$): 311.1866, Found: 311.1864.

5.1.3. 4-[(Adamantan-1-yl)amino]-1*H*-pyrrolo[2,3-*b*]pyridine-5-carboxamide (7c)

A mixture of **6** (40 mg, 0.20 mmol) and 1-adamantylamine (247 mg, 1.64 mmol) in NMP (0.40 mL) was heated in a microwave reactor at 200 °C for 2 h. After cooling to room temperature, H_2O was added and the mixture was extracted with EtOAc. The organic layer was separated, washed with brine, dried over $MgSO_4$, and concentrated under reduced pressure. The residue was purified by column chromatography on silica gel ($CHCl_3$/MeOH =98/2 to 92/8) to give the title compound (40 mg, 63%). ^{1}H NMR (DMSO-d_6) δ 1.63–1.75 (m, 6H), 2.02–2.07 (m, 6H), 2.09–2.15 (m, 3H), 6.66–6.70 (m, 1H), 6.93–7.14 (br, 1H),

7.14–7.20 (m, 1H), 7.65–7.93 (br, 1H), 8.33 (s, 1H), 9.70 (s, 1H), 11.45 (br s, 1H); MS (ESI) *m/z* 311 $[M+H]^+$; HRMS (ESI) *m/z* Calcd for $C_{18}H_{23}N_4O$ ($[M+H]^+$): 311.1866, Found: 311.1865.

5.1.4. Benzyl [(1*R*,2*s*,3*S*,5*s*,7*s*)-5-hydroxyadamantan-2-yl]carbamate (9) and benzyl [(1*R*,2*r*,3*S*,5*s*,7*s*)-5-hydroxyadamantan-2-yl]carbamate (10)

To a solution of 4-aminoadamantan-1-ol (**8**) (8.94 g, 53.5 mmol) in THF (89 mL) were added benzyloxycarbonyl chloride (7.63 mL, 53.5 mmol) and 1 M NaOH aqueous solution (53.5 mL, 53.5 mmol) dropwise successively at 0 °C, and the mixture was stirred for 3 h under the same conditions. The reaction solution was poured into $KHSO_4$ aqueous solution, and the mixture was extracted with EtOAc. The organic layer was washed with brine, dried over $MgSO_4$, and concentrated under reduced pressure. The residue was purified by column chromatography on silica gel (*n*-hexane/EtOAc = 50/50 to 25/75) to give the title compounds **9** (6.2 g, 38%) and **10** (5.3 g, 33%). **9**; ^{1}H NMR (DMSO-d_6) δ 1.22–1.29 (m, 2H), 1.54–1.68 (m, 6H), 1.82–1.97 (m, 5H), 3.52–3.57 (m, 1H), 4.39 (s, 1H), 5.02 (s, 2H), 7.22–7.39 (m, 6H); MS (ESI) *m/z* 324 $[M+Na]^+$. **10**; ^{1}H NMR (DMSO-d6) δ 1.28–1.35 (m, 2H), 1.52–1.60 (m, 6H), 1.81–1.89 (m, 2H), 1.94–2.00 (m, 1H), 2.01–2.07 (m, 2H), 3.40–3.44 (m, 1H), 4.28 (s, 1H), 5.01 (s, 2H), 7.19–7.27 (m, 1H), 7.28–7.40 (m, 5H); MS (ESI) *m/z* 324 $[M+Na]^+$.

5.1.5. (1*s*,3*R*,4*s*,5*S*,7*s*)-4-Aminoadamantan-1-ol (11)

To a solution of **9** (247 mg, 0.82 mmol) in MeOH (5 mL) was added 10% palladim on carbon (50% wet) (87 mg, 0.08 mmol), and the reaction mixture was stirred at room temperature for 5 h under hydrogen atmosphere. After 10% palladim on carbon was filtered off with Celite, the filtrate was concentrated under reduced pressure to give the title compound (135 mg, 98%), which was used in the next reaction without further purification. ^{1}H NMR (CD_3OD) δ 1.39–1.46 (m, 2H), 1.70–1.81 (m, 6H), 1.90–1.98 (m, 4H), 2.03–2.08 (m, 1H), 2.93–2.98 (m, 1H); MS (ESI) *m/z* 168 $[M+H]^+$.

5.1.5. (1*s*,3*R*,4*r*,5*S*,7*s*)-4-Aminoadamantan-1-ol (12)

The title compound was prepared from **10** according to the procedure for preparing **11** in quantitative yield. ^{1}H NMR (DMSO-d_6) δ 1.20–1.33 (m, 2H), 1.46–1.60 (m, 6H), 1.76–1.85 (m, 2H), 1.87–2.01 (m, 3H), 2.68–2.73 (m, 1H), 2.73–3.50 (m, 3H); MS (ESI) *m/z* 168 $[M+H]^+$.

5.1.6. Benzyl [(1*R*,2*s*,3*S*,5*s*,7*s*)-5-fluoroadamantan-2-yl]carbamate (13)

To a solution of **9** (1.0 g, 3.32 mmol) in dichloromethane (10 mL) was added Deoxo-Fluor (808 mg, 3.65 mmol) at 0 °C. After stirring for 0.5 h under the same conditions, the reaction mixture was poured into saturated $NaHCO_3$ aqueous

solution and extracted with EtOAc. The organic layer was washed with H_2O and brine, dried over $MgSO_4$, and concentrated under reduced pressure. The residue was purified by column chromatography on silica gel (*n*-hexane/EtOAc = 92/8 to 80/20) to give the title compound (867 mg, 86%). ^{1}H NMR ($CDCl_3$) δ 1.46–1.53 (m, 2H), 1.65–1.75 (m, 2H), 1.88–1.95 (m, 4H), 1.98–2.08 (m, 2H), 2.17–2.25 (m, 3H), 3.76–3.86 (m, 1H), 4.89–5.01 (m, 1H), 5.10 (s, 2H), 7.30–7.40 (m, 5H); MS (ESI) *m/z* 326 $[M+Na]^+$.

5.1.7. (1*R*,2*s*,3*S*,5*s*,7*s*)-5-Fluoroadamantan-2-amine (14)

The title compound was prepared from **13** according to the procedure for preparing **11** in 89% yield. ^{1}H NMR ($CDCl_3$) δ 1.37–1.44 (m, 2H), 1.77–1.84 (m, 2H), 1.87–2.03 (m, 10H), 2.16–2.23 (m, 1H), 3.05–3.09 (m, 1H); MS (ESI) *m/z* 170 $[M+H]^+$.

5.1.8. Benzyl [(1*R*,2*s*,3*S*,5*s*,7*s*)-5-methoxyadamantan-2-yl]carbamate (15)

To a solution of **9** (4.0 g, 13.3 mmol) in DCE (40 mL) were added trimethyloxonium tetrafluoroborate (3.93 g, 26.5 mmol) and 2,6-di-*tert*-butyl-4-methylpyridine (6.81 g, 33.2 mmol) at room temperature. The reaction mixture was stirred at 95 °C for 2 h. After cooling to room temperature,

the reaction mixture was concentrated under reduced pressure. To the residue was added EtOAc, and the insoluble matter was filtered off. To the filtrate was added H_2O, and the mixture was extracted with EtOAc. The organic layer was washed with H_2O, dried over $MgSO_4$, and concentrated under reduced pressure. The residue was purified by column chromatography on silica gel (*n*-hexane/EtOAc = 90/10 to 70/30) to give the title compound (1.8 g, 43%). ^{1}H NMR (DMSO-d_6) δ 1.25–1.32 (m, 2H), 1.62–1.74 (m, 6H), 1.86–1.93 (m, 2H), 1.96–2.02 (m, 3H), 3.09 (s, 3H), 3.54–3.60 (m, 1H), 5.02 (s, 2H), 7.12–7.40 (m, 6H); MS (ESI) *m/z* 316 $[M+H]^+$.

5.1.9. (1*R*,2*s*,3*S*,5*s*,7*s*)-5-Methoxyadamantan-2-amine (16)

The title compound was prepared from **15** according to the procedure for preparing **11** in 97% yield. ^{1}H NMR (DMSO-d_6) δ 1.37–1.44 (m, 2H), 1.64–1.78 (m, 6H), 1.89–1.96 (m, 2H), 2.04–2.10 (m, 1H), 2.12–2.18 (m, 2H), 3.10 (s, 3H), 3.25–3.28 (m, 1H), 8.06 (br s, 2H); MS (ESI) *m/z* 182 $[M+H]^+$.

5.1.10. 4-{[(1*R*,2*s*,3*S*,5*s*,7*s*)-5-Hydroxyadamantan-2-yl]amino}-1*H*-pyrrolo[2,3-*b*]pyridine-5-carboxamide (17a)

Under a nitrogen atmosphere, a mixture of **6** (2.5 g, 12.8 mmol), **11** (3.2 g, 19.2 mmol) and *n*-Bu_3N (9.1 mL, 38.3 mmol) in NMP (12.5 mL) was stirred at a bath temperature of 200 °C for 2.5 h. After cooling to room temperature, the reaction solution was added dropwise to H_2O/Et_2O while stirring. The obtained solid was collected by filtration, washed with H_2O and Et_2O, and then dried. The obtained solid was warmed and dissolved in MeOH, and filtered while warming. The filtrate was concentrated under reduced pressure. To the residue was added MeOH, and the mixture was heated and dissolved. After cooling to room temperature, the solution was stirred overnight at room temperature. The precipitated solid was collected by filtration, washed MeOH, and dried under reduced pressure to give the title compound (2.1 g, 50%). ^{1}H NMR (DMSO-d_6) δ 1.37–1.46 (m, 2H), 1.62–1.73 (m, 4H), 1.80–1.89 (m, 4H), 2.02–2.08 (m, 1H), 2.12–2.18 (m, 2H), 4.10–4.17 (m, 1H), 4.51 (s, 1H), 6.41 (d, J = 3.6 Hz, 1H), 6.88–7.10 (br, 1H), 7.13 (d, J = 3.6 Hz, 1H), 7.65–7.90 (br, 1H), 8.38 (s, 1H), 10.10 (d, J = 8.0 Hz, 1H), 11.45 (br s, 1H); MS (ESI) *m/z* 327 $[M+H]^+$; Anal. Calcd for $C_{18}H_{22}N_4O_2 \cdot H_2O$: C, 62.77; H, 7.02; N, 16.27. Found: C, 62.39; H, 7.04; N, 16.14.

5.1.11.

4-{[(1*R*,2*r*,3*S*,5*s*,7*s*)-5-Hydroxyadamantan-2-yl]amino}-1*H*-pyrrolo[2,3-*b*]pyridine-5-carboxamide (17b)

The title compound was prepared from **6** according to the procedure for preparing **17a** in 49% yield. ^{1}H NMR (DMSO-d_6) δ 1.40–1.48 (m, 2H), 1.57–1.71 (m, 4H), 1.73–1.90 (m, 4H), 2.03–2.10 (m, 1H), 2.18–2.25 (m, 2H), 3.99–4.06 (m, 1H), 4.49 (s, 1H), 6.43 (d, J = 3.6 Hz, 1H), 6.82–7.16 (br, 1H), 7.11 (d, J = 3.6 Hz, 1H), 7.56–7.90 (br, 1H), 8.37 (s, 1H), 10.12 (d, J = 8.0 Hz, 1H), 11.43 (br s, 1H); MS (ESI) *m/z* 327 $[M+H]^+$; Anal. Calcd for $C_{18}H_{22}N_4O_2 \cdot H_2O$: C, 62.77; H, 7.02; N, 16.27. Found: C, 62.64; H, 7.03; N, 16.26.

5.1.12.

4-{[(1*R*,2*s*,3*S*,5*s*,7*s*)-5-Fluoroadamantan-2-yl]amino}-1*H*-pyrrolo[2,3-*b*]pyridine-5-carboxamide (17c)

The title compound was prepared from **6** according to the procedure for preparing **7b** in 65% yield. ^{1}H NMR (DMSO-d_6) δ 1.44–1.50 (m, 2H), 1.82–1.93 (m, 6H), 2.11–2.22 (m, 3H), 2.24–2.29 (m, 2H), 4.21–4.26 (m, 1H), 6.47–6.50 (m, 1H), 6.88–7.16 (m, 2H), 7.63–7.93 (br, 1H), 8.38 (s, 1H), 10.10 (d, J = 8.0 Hz,

1H), 11.46 (br s, 1H); MS (ESI) *m/z* 329 $[M+H]^+$; HRMS (ESI) *m/z* Calcd for $C_{18}H_{22}N_4OF$ ($[M+H]^+$): 329.1772, Found: 329.1763.

5.1.13.

4-{[(1*R*,2*s*,3*S*,5*s*,7*s*)-5-Methoxyadamantan-2-yl]amino}-1*H*-pyrrolo[2,3-*b*]pyridine-5-carboxamide (17d)

The title compound was prepared from **6** according to the procedure for preparing **7b** in 37% yield. ^{1}H NMR (DMSO-d_6) δ 1.40–1.48 (m, 2H), 1.68–1.78 (m, 4H), 1.82–1.98 (m, 4H), 2.07–2.13 (m, 1H), 2.17–2.23 (m, 2H), 3.15 (s, 3H), 4.13–4.20 (m, 1H), 6.43–6.48 (m, 1H), 6.86–7.16 (m, 2H), 7.57–7.91 (br, 1H), 8.37 (s, 1H), 10.11 (d, *J* = 8.0 Hz, 1H), 11.43 (br s, 1H); MS (ESI) *m/z* 341 $[M+H]^+$; HRMS (ESI) *m/z* Calcd for $C_{19}H_{25}N_4O_2$ ($[M+H]^+$): 341.1972, Found: 341.1971.

5.1.14.

4-{[(1*R*,2*s*,3*S*,5*s*,7*s*)-5-Hydroxyadamantan-2-yl]amino}-1*H*-pyrrolo[2,3-*b*]pyridine-5-carboxamide monohydrobromide (18)

48% hydrobromic acid (258 μL, 1.53 mmol) was added to a suspension of **17a** (500 mg, 1.53 mmol) in EtOAc (25 mL) at room temperature. The reaction

mixture was refluxed for 1 h. After cooling to room temperature, the precipitated crystals were collected by filtration and washed with EtOAc. The obtained crystals were dried at 60°C under reduced pressure to give the title compound (625 mg, quantitative yield). ^{1}H NMR (DMSO-d_6) δ 1.45–1.53 (m, 2H), 1.64–1.74 (m, 4H), 1.75–1.84 (m, 2H), 1.86–1.95 (m, 2H), 2.06–2.12 (m, 1H), 2.16–2.23 (m, 2H), 3.16–3.82 (br, 1H), 4.22–4.31 (m, 1H), 6.64–6.67 (m, 1H), 7.37–7.41 (m, 1H), 7.74 (br s, 1H), 8.35 (br s, 1H), 8.52 (s, 1H), 11.15 (d, J = 8.0 Hz, 1H), 12.48 (s, 1H), 14.13 (br s, 1H); MS (ESI) *m/z* 327 $[M+H]^+$; Anal. Calcd for $C_{18}H_{22}N_4O_2 \cdot HBr$: C, 53.08; H, 5.69; N, 13.76; Br, 19.62. Found: C, 53.04; H, 5.69; N, 13.68; Br, 19.63.

5.2. Computational analysis

5.2.1. Docking calculation

Docking calculation was performed on the crystal structure of tofacitinib (**1**) bound to JAK3 (PDB code: 3LXK[32]). The protein-ligand complex was prepared using the Protein Preparation Wizard in Maestro 9.3 (Schrödinger, LLC, New York, NY, 2012) with the Impref Module to apply the appropriate side-chain protonation states, refine, and minimize the structure. Docking grids were generated and defined based on the centroid of tofacinitib in the ATP-binding site,

incorporating hydrogen-bond constraints to the hinge region and hydrophobic region constraints. Ligand was prepared using LigPrep 2.5 and Confgen 2.3 (Schrödinger, LLC, New York, NY, 2012), and the energy-minimized conformation of each ligand was used to docking calculation input molecule. Ligand receptor docking was carried out using XP mode in Glide 5.8 (Schrödinger, LLC, New York, NY, 2012). The top scoring pose, as assessed by the Glidescore, was employed for discussion.

5.2.2. WaterMap analysis

WaterMap (Schrödinger Release 2016-1: Schrödinger, LLC, New York, NY, 2016) calculations were conducted on the co-crystal structures of peficitinib (ASP015K) bound to JAK1, JAK2, JAK3, and TYK2 by preparing the protein-ligand structure using the Protein Preparation Wizard in Maestro (Schrödinger Release 2016-1). WaterMap was run in default mode with OPLS_2005 forcefield, existing waters deleted, and a 2 ns MD simulation. The peficitinib structure was used to define the binding site but was removed in the MD simulation.

5.3. Biology

5.3.1. Human JAK kinase assay

Human JAK1, JAK2, and JAK3 kinase domains were purchased from Carna Biosciences, Inc. (Kobe, Japan), and the assay was performed using a streptavidin-coated 96-well plate. The reaction mixture contained 15 mM Tris-HCl (pH 7.5), 0.01% Tween 20, 2 mM DTT, 10 mM $MgCl_2$, 250 nM Biotin-Lyn-Substrate-2 (Peptide Institute, Inc., Osaka, Japan) and ATP. The final concentrations of ATP were 200, 10, and 8 μM for JAK1, JAK2, and JAK3, respectively. Test compounds were dissolved in DMSO and the reaction was initiated by adding the kinase domain, followed by incubation at room temperature for 1 h. Kinase activity was measured as the rate of phosphorylation of Biotin-Lyn-Substrate-2 using HRP-conjugated anti-phosphotyrosine antibody (HRP-PY-20; Santa Cruz Biotechnology, Inc., Santa Cruz, CA, USA) with a phosphotyrosine-specific ELISA. The TYK2 kinase assay of **18** was performed at Carna Biosciences, Inc., with the ATP concentration modified to 10 μM. All experiments were performed in duplicate. The IC_{50} value of all compounds except for **18** was calculated using linear regression analysis. The IC_{50} value of **18** was calculated using Sigmoid-Emax non-linear regression analysis, and expressed as the mean and 95% confidence interval of four independent experiments.

5.3.2. Rat T cell proliferation

Splenocytes from male Lewis rats were suspended in RPMI1640 (Sigma, St. Louis, MO, USA) supplemented with 10% fetal bovine serum and 50 μM 2-mercaptoethanol at a density of 1.5 $\times 10^6$ cells/mL. Rat splenocytes were cultured with concanavalin A (Sigma) for 24 h at 37°C to induce IL-2 receptor expression. Splenocytes were then incubated with IL-2 (BD Biosciences, San Diego, CA, USA) and test compounds at designated concentrations in 96-well tissue culture plates. After incubation for 3 days, alamarBlue® (Life Technologies, Carlsbad, CA, USA) was added to each of the test wells, followed by incubation for 6 h. Fluorescence intensity was measured at an excitation wavelength of 545 nm and an emission wavelength of 590 nm. The experiment was performed in duplicate for **5**, and the IC_{50} value of **5** was calculated using linear regression analysis. The experiment was performed in triplicate for **18**, and the IC_{50} value of **18** was calculated using Sigmoid-Emax non-linear regression analysis, and expressed as the mean and 95% confidence interval of four independent experiments. All animal experimental procedures were approved by the Institutional Animal Care and Use Committee of Astellas Pharma Inc.

5.3.3. Human T cell proliferation

Human peripheral blood mononuclear cells (hPBMCs) from healthy volunteers were isolated using a Ficoll gradient, and suspended in RPMI1640 supplemented 10% fetal bovine serum, 100 U/mL penicillin, and 100 μg/mL streptomycin (culture medium) at a density of 5×10^5 cells/mL. Human PBMCs were cultured with 10 μg/mL phytohemagglutinin (Sigma) for 5 days at 37°C, 5% CO_2. After washing, 2×10^4 hPBMCs were incubated with 1 ng/mL IL-2 (BD Biosciences, San Diego, CA, USA) and **18** at designated concentrations in 96-well tissue culture plates. After incubation for 3 days, cell proliferation was quantified using alamarBlue® as described above. The assay was performed in triplicate for each set of conditions. For each individual, blanks and controls were designated as 100% and 0% inhibition, respectively. The IC_{50} value of **18** was calculated using Sigmoid-Emax non-linear regression analysis, and expressed as the mean and 95% confidence interval of four independent experiments. All studies using human materials were approved by the Astellas Research Ethics Committee and all human material was obtained from healthy donors who provided written informed consent.

5.3.4. Human erythroleukemia cell line TF-1 proliferation

TF-1 cells, obtained from the American Type Culture Collection (Manassas, VA, USA), were maintained in culture medium supplemented with 2 ng/mL of GM-CSF (IBL, Gunma, Japan). Before the experiments, TF-1 cells were deprived of GM-CSF by washing with RPMI1640 and incubating overnight in culture medium. For the experiments, 2.5×10^4 TF-1 cells were incubated with 1 U/mL EPO (Kirin Brewery, Tokyo, Japan) and **18** at designated concentrations in 96-well microplates for 2 days at 37°C, 5% CO_2. Cell proliferation was quantified by using alamarBlue® as described above. The experiment was performed in triplicate. Blanks and controls were designated as 100% and 0% inhibition, respectively. The IC_{50} value of **18** was calculated using Sigmoid-Emax non-linear regression analysis, and expressed as the mean and 95% confidence interval of four independent experiments.

5.3.5. In vitro liver microsomal stability

To estimate stability against rat hepatic CYPs, test compound (0.2 or 1.0 μM) was incubated with male SD rat liver microsomes or male/female human liver microsomes (0.2 mg protein/mL) in the presence of NADPH (1 mM) and EDTA

(0.1 mM) in phosphate buffer (100 mM) at 37°C. The percentage of compound remaining was determined by LC/MS/MS.

5.3.6. Pharmacokinetic study

Pharmacokinetic characterization of compound **18** was conducted in male SD rats [Sprague-Dawley strain SPF rats Crl:CD(SD), 7 weeks of age]. Compound **18** was orally administered at 1 mg/kg in 0.5 w/v% methylcellulose solution, and intravenously at 1 mg/kg in 10 v/v% propylene glycol solution. The animals were food deprived prior to administration. Blood samples were collected at multiple time-points up to 24 h after a single administration of compound **18**. The plasma concentrations of the unchanged compound were determined by LC/MS/MS, and the PK parameters were calculated.

Acknowledgements

The authors thank Dr. Kazuo Oda for evaluating the compounds, and Dr. Yukihiro Tateishi and Mr. Yusuke Tomimoto for providing the recombinant proteins. The authors also thank Mr. Hiroyuki Kaizawa, Mr. Hiroaki Yamagishi, and Dr. Tatsuya Niimi for their support in the preparation of this manuscript. In addition, the authors are grateful to the staff of the Division of Analytical Science Laboratories for conducting elemental analysis and spectral measurements.

References

1. Smolen, J. S.; Aletaha, D.; Mclnnes, I. B. *Lancet* **2016**, *388*, 2023.
2. Moelants, E. A.; Mortier, A.; Damme, J. V.; Proost, P. *Immunol. Cell Biol.* **2013**, *91*, 393.
3. Smolen, J. S.; Beaulieu, A.; Rubbert-Roth, A.; Ramos-Remus, C.; Rovensky, J.; Alecock, E.; Woodworth, T.; Alten, R. *Lancet* **2008**, *371*, 987.
4. Mok, C. C.; Tsai, W. C.; Chen, D. Y.; Wei, J. C. C. *Expert Opin. Biol. Ther.* **2016**, *16*, 201.
5. Cheung, T. T.; McInnes, I. B. *Semin. Immunopathol.* **2017**, *39*, 487.
6. Rivellese F.; Lobasso A.; Barbieri L.; Liccardo B.; De Paulis A.; Rossi F. W. *Curr. Med. Chem.* **2018** Feb 9. [Epub ahead of print] *doi:10.2174/0929867325666180209145243*
7. Imada, K.; Leonard, W. J. *Mol. Immunol.* **2000,** *37*, 1.
8. Leonard, W. J.; Lin, J. X. *J. Allergy Clin. Immunol.* **2000,** *105*, 877.
9. Shuai, K.; Liu, B. *Nat. Rev. Immunol.*, **2003**, *3*, 900.
10. O'Shea, J. J.; Pesu, M.; Borie, D. C.; Changelian, P. S. *Nat. Rev. Drug Discov.* **2004,** *3*, 555.
11. Ghoreschi, K.; Laurence, A.; O'Shea, J. J. *Immunol. Rev.* **2009,** *228*, 273.

12. O'Shea, J. J.; Plenge, R. *Immunity* **2012,** *36*, 542.

13. Johnston, J. A.; Kawamura, M.; Kirken, R. A.; Chen, Y. Q.; Blake, T. B.; Shibuya, K.; Ortaldo, J. R.; McVicar, D. W.; O'Shea, J. J. *Nature* **1994,** *370*, 151.

14. Witthuhn, B. A.; Silvennoinen, O.; Miura, O.; Lai, K. S.; Cwik, C.; Liu, E. T.; Ihle, J. N. *Nature* **1994,** *370*, 153.

15. Yamaoka, K.; Saharinen, P.; Pesu, M.; Holt III, V. E. T.; Silvennoinen, O.; O'Shea, J. J. *Genome Biol.* **2004**, *5*, 253.

16. Nosaka, T.; van Deursen, J. M. A.; Tripp, R. A.; Thierfelder, W. E.; Witthuhn, B. A.; McMickle, A. P.; Doherty, P. C.; Grosveld, G. C.; Ihle, J. N. *Science* **1995,** *270*, 800.

17. Park, S. Y.; Saijo, K.; Takahashi, T.; Osawa, M.; Arase, H.; Hirayama, N.; Miyake, K.; Nakauchi, H.; Shirasawa, T.; Saito, T. *Immunity* **1995,** *3*, 771.

18. Broxmeyer, H. E. *J. Exp. Med*. **2013**, *210*, 205.

19. Ishizaki M.; Muromoto R.; Akimoto T.; Sekine Y.; Kon S.; Diwan M.; Maeda H.; Togi S.; Shimoda K.; Oritani K.; Matsuda T. *Int. Immunol.* **2014**, *26*, 257.

20. Liang J,; Tsui V.; Van Abbema A.; Bao L.; Barret K.; Beresini M.; Berezhkovskiy L.; Blair W. S.; Chang C.; Driscoll J.; Eigenbrot C.; Ghilardi

N.; Gibbons P.; Halladay J.; Johnson A., Kohli P. B.; Lai Y.; Liimatta M.; Mantik P.; Menghrajani K.; Murray J.; Sambrone A.; Xiao Y,; Shia S.; Shin Y.; Smith J.; Sohn S.; Stanley M.; Ultsch M.; Zhang B.; Wu L. C.; Magnuson S. *Eur. J. Med. Chem*. **2013**, *67*, 175.

21. Norman, P. *Expert Opin. Investig. Drugs.* **2014**, *23*, 1067.

22. Semerano, L.; Decker, P.; Clavel G.; Boissier M. C. *Expert Opin. Investig. Drugs.* **2016**, *25*, 1355.

23. Flanagan, M. E.; Blumenkopf, T. A.; Brissette, W. H.; Brown, M. F.; Casavant, J. M.; Shang-Poa, C.; Doty, J. L.; Elliott, E. A.; Fisher, M. B.; Hines, M.; Kent, C.; Kudlacz, E. M.; Lillie, B. M.; Magnuson, K. S.; McCurdy, S. P.; Munchhof, M. J.; Perry, B. D.; Sawyer, P. S.; Strelevitz, T. J.; Subramanyam, C.; Sun, J.; Whipple, D. A.; Changelian, P. S. *J. Med. Chem.* **2010,** *53*, 8468.

24. Clark, J. D.; Flanagan, M. E.; Telliez, J. B. *J. Med. Chem.* **2014,** *57*, 5023.

25. Markham, A. *Drugs* **2017**, *77*, 697.

26. Westhovens, R.; Taylor, P. C.; Alten, R.; Pavlova, D.; Enríquez-Sosa, F.; Mazur, M.; Greenwald, M.; Van der Aa, A.; Vanhoutte, F.; Tasset, C.; Harrison, P. *Ann. Rheum. Dis.* **2017,** *76*, 998.

27. Genovese, M. C.; Smolen, J. S.; Weinblatt, M. E.; Burmester, G. R.; Meerwein, S.; Camp, H. S.; Wang, L.; Othman, A. A.; Khan, N.; Pangan, A. L.; Jungerwirth, S. *Arthritis Rheum.* **2016,** *68*, 2857.

28. Nakajima, Y.; Tojo, T.; Morita, M.; Hatanaka, K.; Shirakami, S.; Tanaka, A.; Sasaki, H.; Nakai, K.; Mukoyoshi, K.; Hamaguchi, H.; Takahashi, F.; Moritomo, A.; Higashi, Y.; Inoue, T. *Chem. Pharm. Bull.* **2015**, *63*, 341.

29. Lavrova, L. N.; Indulen, M. K.; Ryazantseva, G. M.; Korytnyi, V. S.; Yashunskii, V. G. *Pharm. Chem. J.* **1990,** *24*, 35.

30. Jaroskova, L.; Van der Veken, L.; de Belser, P.; Diels, G.; de Groot, A.; Linders, J. T. M. *Tetrahedron Lett.* **2006,** *47*, 8063.

31. Neubauer, H.; Cumano, A.; Muller, M.; Wu, H.; Huffstadt, U.; Pfeffer, K. *Cell* **1998,** *93*, 397.

32. Chrencik, J. E.; Patny, A.; Leung, I. K.; Korniski, B.; Emmons, T. L.; Hall, T.; Weinberg, R. A.; Gormley, J. A.; Williams, J. M.; Day, J. E.; Hirsch, J. L.; Kiefer, J. R.; Leone, J. W.; Fischer, H. D.; Sommers, C. D.; Huang, H. C.; Jacobsen, E. J.; Tenbrink, R. E.; Tomasselli, A. G.; Benson, T. E. *J. Mol. Biol.* **2010,** *400*, 413.

33. Ito, M.; Yamazaki, S.; Yamagami, K.; Kuno, M.; Morita, Y.; Okuma, K.; Nakamura, K.; Chida, N.; Inami, M.; Inoue, T.; Shirakami, S.; Higashi, Y.; *J. Pharmacol. Sci.* **2017**, *133*, 25.

34. Abel, R.; Young, T.; Farid, R.; Berne, B. J.; Friesner, R.A., *J. Am. Chem. Soc.* **2008**, *130*, 2817.

35. Young, T.; Abel, R.; Kim, B.; Berne, B.J.; Friesner, R.A., *Proc. Natl. Acad. Sci. U S A.* **2007**, *104*, 808.

36. X-ray crystal structures of JAK1 and JAK3 were determined by Proteros biostructures GmbH (Martinsried, Germany)

Graphical abstract

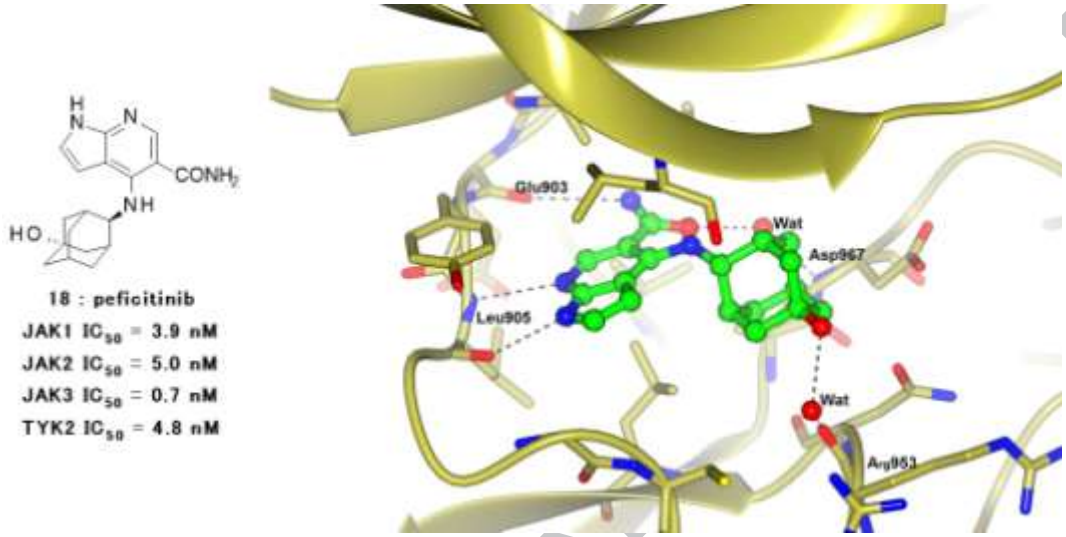

37.